J Neurophysiol 118: 2853–2864, 2017.
First published August 23, 2017; doi:10.1152/jn.00061.2017.

RESEARCH ARTICLE | *Neural Circuits*

Intrinsic frequency biases and profiles across human cortex

Monika S. Mellem,[1] Sophie Wohltjen,[1] Stephen J. Gotts,[1] Avniel Singh Ghuman,[1,2] and Alex Martin[1]
[1]*Section on Cognitive Neuropsychology, Laboratory of Brain and Cognition, National Institute of Mental Health, National Institutes of Health, Bethesda, Maryland; and* [2]*Department of Neurological Surgery, University of Pittsburgh Medical Center, Pittsburgh, Pennsylvania*

Submitted 30 January 2017; accepted in final form 22 August 2017

Mellem MS, Wohltjen S, Gotts SJ, Ghuman AS, Martin A. Intrinsic frequency biases and profiles across human cortex. *J Neurophysiol* 118: 2853–2864, 2017. First published August 23, 2017; doi:10.1152/jn.00061.2017.—Recent findings in monkeys suggest that intrinsic periodic spiking activity in selective cortical areas occurs at timescales that follow a sensory or lower order-to-higher order processing hierarchy (Murray JD, Bernacchia A, Freedman DJ, Romo R, Wallis JD, Cai X, Padoa-Schioppa C, Pasternak T, Seo H, Lee D, Wang XJ. *Nat Neurosci* 17: 1661–1663, 2014). It has not yet been fully explored if a similar timescale hierarchy is present in humans. Additionally, these measures in the monkey studies have not addressed findings that rhythmic activity within a brain area can occur at multiple frequencies. In this study we investigate in humans if regions may be biased toward particular frequencies of intrinsic activity and if a full cortical mapping still reveals an organization that follows this hierarchy. We examined the spectral power in multiple frequency bands (0.5–150 Hz) from task-independent data using magnetoencephalography (MEG). We compared standardized power across bands to find regional frequency biases. Our results demonstrate a mix of lower and higher frequency biases across sensory and higher order regions. Thus they suggest a more complex cortical organization that does not simply follow this hierarchy. Additionally, some regions do not display a bias for a single band, and a data-driven clustering analysis reveals a regional organization with high standardized power in multiple bands. Specifically, theta and beta are both high in dorsal frontal cortex, whereas delta and gamma are high in ventral frontal cortex and temporal cortex. Occipital and parietal regions are biased more narrowly toward alpha power, and ventral temporal lobe displays specific biases toward gamma. Thus intrinsic rhythmic neural activity displays a regional organization but one that is not necessarily hierarchical.

NEW & NOTEWORTHY The organization of rhythmic neural activity is not well understood. Whereas it has been postulated that rhythms are organized in a hierarchical manner across brain regions, our novel analysis allows comparison of full cortical maps across different frequency bands, which demonstrate that the rhythmic organization is more complex. Additionally, data-driven methods show that rhythms of multiple frequencies or timescales occur within a particular region and that this nonhierarchical organization is widespread.

cortical rhythms; EEG/MEG; spectral analysis; clustering

TO UNDERSTAND THE FUNCTIONAL ROLES of brain rhythms, a common approach has been to relate cognitive and motor tasks to modulation of activity in specific frequency bands (or at specific timescales). A far less common but promising approach has been to examine spontaneous rhythmic activity and its organization across functionally specialized regions of the brain. The implications of outlining a fundamental organization of timescales in the brain are far-reaching, including potentially furthering our understanding of how incoming information over time is combined into complex representations (Hasson et al. 2015; Kiebel et al. 2008) and of how interregional connectivity depends on frequency in typically developing brains (Engel et al. 2001; Fries 2015; Palva and Palva 2011; Singer 2013) and disordered states (Eggermont and Tass 2015; Uhlhaas 2013).

Recent findings in nonhuman primates have examined intrinsic timescales and suggest that intrinsic periodic spiking activity occurs on different timescales across cortical regions (Murray et al. 2014). In recording spiking activity from seven regions, collected over six data sets, the organization of these timescales was found to follow a rough anatomically defined hierarchy such that activity in sensory regions occurred at faster timescales (~50–150 ms) whereas activity in higher order regions occurred at slower timescales (~50–350 ms).

It is not clear, however, how this proposal can account for findings from both monkey and human electrophysiology studies showing that rhythms within a region occur at multiple timescales (Buffalo et al. 2011; Heusser et al. 2016; Keitel and Gross 2016; Mantini et al. 2007; van Kerkoerle et al. 2014). For example, both gamma and alpha rhythms are observed in visual cortex (Lozano-Soldevilla et al. 2014; Michalareas et al. 2016; Sellers et al. 2015), although they may be segregated by cortical layer (Buffalo et al. 2011; van Kerkoerle et al. 2014; Xing et al. 2012). These concerns suggest that an approach of comparing power across different frequency bands to find a frequency bias may help us evaluate this hierarchy proposal more comprehensively than the autocorrelation approach previously taken (Murray et al. 2014). Additionally, a fuller evaluation of the hierarchy proposal necessitates examining a larger set of brain regions, ideally the full cortex. Although some studies have examined electrophysiological timescales of operation, they are limited in focus on visual cortex (Gauthier et al. 2012), on resting-state networks defined by MRI blood oxygen level-dependent (BOLD) fluctuations (Mantini et al. 2007), and on placement of electrocorticographic (ECoG) subdural electrodes (He et al. 2008). Thus our unconstrained, whole brain approach is able to more comprehensively evalu-

Address for reprint requests and other correspondence: M. S. Mellem, Bldg. 10, Rm. 4C-104 MSC-1366, Bethesda, MD 20892-1366 (e-mail: monikamellem@gmail.com).

ate a timescale hierarchy. It also is not yet known if a similar timescale hierarchy is present in humans. For these reasons, we took the approach of studying human subjects with magnetoencephalography (MEG), which can give a full cortical mapping.

Our two main questions with this study are *1*) Does the hierarchical organization of timescales hold if we examine the whole cortex in humans? and *2*) If it does not hold, what is the relationship between rhythmic neural activity and cortical region? Answering these questions involved the use of both hypothesis-driven and data-driven analyses of spontaneous or "resting-state" MEG. To answer the first question, we developed a novel approach to spectral power analysis. Specifically, power across different frequency bands must be compared to test for a frequency bias for a given region, but power decays from lower to higher frequencies with a 1/*f* slope (Buzsáki 2006). Because each rhythm is relevant to neural processing on its own scale (i.e., delta operates in the brain on a very different scale from gamma, but both are relevant), we estimated each frequency band's scale from cortical source estimates and standardized each band's power in each region. Comparisons of standardized power across the spectrum revealed a cortical organization of timescales that cannot simply be explained by a hierarchy with biases to a single frequency band. Our statistical approach for comparing frequencies is key to addressing the hierarchy question and has not been done before to our knowledge. To address the second question, we used a clustering approach to elucidate the general spectral profiles of cortical regions and how multiple frequency bands may be grouped.

MATERIALS AND METHODS

Subjects. Thirty-three subjects participated in the study. Two subjects were excluded due to excessive head motion, and one was excluded for a MEG recording irregularity during the scan that rendered the scan unusable. Thus 30 subjects remained in all subsequent analysis (9 women; mean age 25.1 yr, SD 5.1 yr). All subjects were screened and did not report any neurological or psychiatric problems. Written informed consent was obtained from each subject in accordance with a National Institutes of Health Institutional Review Board-approved protocol. Subjects were paid for their participation.

MEG acquisition. For each subject, whole head MEG was recorded with 275 radial gradiometers (273 of which were functional) at 600 Hz inside a shielded room (VSM MedTech, Coquitlam, BC, Canada). Spontaneous data were collected for 5 or 10 min while subjects fixated on a centrally presented cross. Synthetic third-order gradient noise cancellation was used during each scan. Head position was tracked using coils placed at three fiducial points (the nasion, left and right preauricular points) as recommended by several experts (Hansen et al. 2010; Hari and Puce 2017). Head motion was calculated from the root mean squared maximal displacement across the three fiducial channels, and subjects with >10-mm movements were excluded from further analysis. Of the remaining subjects, the mean maximum motion was 3.1 mm (SD 2.2 mm). An electrooculogram (EOG) was also collected. A bipolar EOG electrode was placed above and at the outer canthus of each subject's left eye to record eyeblinks and eye movements.

Structural MRI acquisition. A 3-Tesla scanner (GE Signa) was used to acquire structural MRIs. A high-resolution T1-weighted whole brain volume was acquired for each subject, and automatic reconstruction in FreeSurfer was used to create each subject's cortical surface model. MEG data and surface models were then aligned using the three fiducial points. The white matter surface of the model was segmented into 150,000 vertices per hemisphere and then decimated to 4,000 source dipoles per hemisphere, spaced ~10 mm apart. Each subject's source space was morphed to FreeSurfer's fsaverage common space using 2,562 dipoles per hemisphere for group-level analysis.

MEG preprocessing. We first visually inspected all data for general data quality and recorded any channels with substantial respiratory artifacts. Artifact removal was done using the FieldTrip MATLAB toolbox (Oostenveld et al. 2011) and custom MATLAB scripts. To remove low-frequency drift, any respiratory artifacts, and any DC offset, we used a fourth-order Butterworth filter to bandpass the data between 0.5 and 150 Hz and two notch filters (forward and reverse Butterworth filter to provide a zero-phase output) at 60 and 120 Hz to remove line noise. We then performed independent components analysis (ICA; Jung et al. 2000) using FieldTrip to decompose the MEG sensor data into 273 independent components (ICs) and subsequently isolate and remove ICs corresponding to eyeblinks, other eye movements, and cardiac artifacts. ICs were identified as being a cardiac artifact if the IC had both regular peaks every 667–1,667 ms in its time series and a peak in its spectrum between 0.6 and 1.5 Hz (mean no. of cardiac ICs removed = 1.67, SD 0.69). Ocular muscle artifact ICs were identified by comparing ICs with EOG time courses. ICs with a typical frontally biased pattern and that had eyeblink artifacts at the same time as artifacts seen in EOG channels were identified as oculomotor artifacts and removed (mean no. of oculomotor ICs removed = 3.06, SD 2.0). Occasionally ICs contained horizontal eye movement artifacts or jump artifacts, and these were removed also. Remaining ICs were reassembled for further analysis.

Because muscle artifacts are prominent in the higher frequencies, we chose to remove them before further analysis of the gamma bands. Visual inspection revealed muscle artifacts that were transient, large-amplitude, high-frequency oscillatory bursts in a subset of subjects. We used a semiautomated *z*-score approach to remove them (implemented in FieldTrip and custom code). Because muscle artifacts most commonly occur in the gamma range, we bandpass filtered the data between 30 and 150 Hz to search for muscle artifacts. The time series of each channel was then *z*-transformed by the mean and SD of that channel. Because muscle artifacts often occur across many channels, a summary *z*-score time course can be obtained by averaging *z* scores sample by sample across the 273 channels. Each sample of the averaged *z*-score time series that exceeded an individually set *z*-score threshold was marked (with 1-s padding on either side), and contiguous samples were inspected in the raw data to confirm the existence of a muscle artifact. If the individual *z*-score threshold identified too few muscle artifacts (true positives) or too many sections without muscle artifacts (false positives), the threshold was adjusted. In a few cases, some very subtle low-amplitude muscle artifacts were left in to avoid removing tens of seconds of clean data. Samples corresponding to the identified muscle artifacts were then automatically removed across all channels, and a five-sample spline interpolation was inserted in each channel's time series to avoid sharp discontinuities in the data. On average, 2.85% (SD 3.16%) of data was removed for muscle artifacts across subjects. Additional steps to investigate associations between gamma activity due to muscle activity and the source-localized gamma were taken. We examined any associations between eye movements and gamma localized to the cortical surface across subjects. Because the EOG provides a separate measurement dominated by ocular muscle movements, we performed spectral analysis of the EOG channel and examined Pearson's correlations between gamma (30–50 Hz) of EOG and each of the 148 regions of interest (ROIs), between high gamma 1 of EOG and all ROIs, and between high gamma 2 and all ROIs. Of these 444 tests, only 2 returned a significant correlation, mainly due to a single outlier: the left and right calcarine sulcus were correlated with high gamma 1 ($\rho = 0.36$, $P = 0.049$; $\rho = 0.37$, $P = 0.045$, respectively). After false discovery rate (FDR) correction for the 444 tests, neither was still significant. Thus

cortical gamma does not seem to be confounded with ocular muscle movements in the current study.

Source analysis allows estimation of the locations and time courses of cortical sources from the magnetic fields measured at the scalp. We used the minimum norm estimate (MNE) distributed source model to approximate the sources of cortical currents (Hämäläinen and Ilmoniemi 1994) simultaneously and the corresponding MNE software toolbox (Gramfort et al. 2014) for the following analysis. The MNE is calculated by finding a linear inverse operator that transforms the measured MEG channel-level data to current sources on the cortical surface. First, a forward model is created that transforms orthogonal unit current dipoles at each vertex to scalp magnetic field projections and is constrained by a boundary element model (Hämäläinen and Sarvas 1989). This, along with noise and source covariance matrices and a weighting factor of 3 to avoid magnification of errors in the data (Hämäläinen 2009; MNE software version 2.7), is used to compute the inverse operator. Ten minutes of empty room MEG data are collected just before each subject's scan and used to calculate the noise covariance matrix (Ghuman et al. 2011), whereas the full 5- to 10-min spontaneous data recording is used for the source covariance matrix and the source projections. Other constraints included a loose orientation constraint where the component of the source covariance matrix normal to the surface is multiplied by 1 and the component transverse is multiplied by 0.4 (because cortical neurons are oriented perpendicular to the cortical surface). The MNE is also biased toward superficial currents, so a depth weighting factor of 0.8 is also applied to compensate (Lin et al. 2004). After each subject's channel time courses were projected onto their individual reconstructed cortical surface, the surface sources were transformed into a common neural space using FreeSurfer's fsaverage brain.

MEG spectral analysis. Spectral power analysis was then used to investigate the timescales of rhythmic activity at each source. The power spectrum is a decomposition of a time series into Fourier components representing the squared amplitude of each frequency component in the time series. In this way, both the power at each frequency, f, and the timescales, or periods ($1/f$), can be estimated from the time series, and the relative contribution of different frequencies can be assessed. For each subject, the first 5 min of the time series at each source-localized vertex were windowed with a Hamming function and power was estimated using a periodogram. Because sources farther from the scalp are weaker and result in weaker spectra primarily from the drop-off of a magnetic field with distance and not from differences in neural processes, the power spectrum of each vertex was normalized over our band of interest, the range from 0.5 to 150 Hz. We also confirmed that both raw and normalized spectra from medial and ventral regions reflected neurophysiological data in that they had a $1/f$ slope, had an alpha bump, and differed significantly from room noise that was projected back through the source model. To summarize power spectra across vertices, we averaged the spectra within each of 148 ROIs from the Destrieux atlas (Destrieux et al. 2010). Each ROI is defined anatomically by gyral and sulcal boundaries. Spectral power was also divided into several typical frequency bands: delta (0.5–4 Hz), theta (4–8 Hz), alpha (8–14 Hz), low beta (14–20 Hz), high beta (20–30 Hz), low gamma (30–50 Hz), high gamma 1 (50–100 Hz), and high gamma 2 (100–150 Hz). The beta band is sometimes examined as a single unit, although in this case we separate it into two, because low- and high-beta bands have been shown to respond differently during deep brain stimulation (Müsch et al. 2017; Oswal et al. 2016). Also, although the higher gamma bands are often not examined because of muscle artifact contamination, we chose to analyze them because they may reflect different types of activity (Crone et al. 2011), and recent results suggest MEG is sensitive to this part of the spectrum (Rutter et al. 2009). In this manner we determined power estimates for each frequency band in each ROI, and these data are available as Supplemental Material in the form of comma-separated values (.csv) files (both grand average and individual subjects). (Supplemental Material for this article is available online at the *Journal of Neurophysiology* website.) Because parametric tests were used at a later stage, we applied a power function to the data (we found $x^{1/6}$ worked well empirically) and tested for normality of each distribution of each frequency band at each ROI using the Lilliefors test (lillietest function in MATLAB). Because the vast majority of these distributions passed the Lilliefors test, we proceeded with parametric statistics for the main analysis. In comparing power across frequency bands to determine dominant timescales or frequencies, we are limited by the typical $1/f$ slope of the neurophysiological power spectrum. For example, whereas power in the lowest part of the delta frequency band (<1 Hz) is commonly the greatest across much of cortex, it can be argued that rhythmic activity at each frequency is relevant while operating on its own scale. For example, although relatively very small, gamma oscillations are involved in processing in visual cortex (Buffalo et al. 2011), whereas delta oscillations are not thought to be consequential in this region. Thus we chose to standardize power separately within each band before making comparisons across frequencies. This was done by estimating the relevant scale of each frequency band by examining power across the 148 ROIs. For each band, the mean and SD of power were calculated across ROIs, and z scores were calculated with these measures to create standardized power measures at each ROI. The standardized power data are also available as Supplemental Material (.csv files; both grand averaged and individual subjects). Robustness of these estimates were demonstrated through interindividual variability and split-cohort reliability calculations. We calculated the interindividual variability by calculating the standard deviation of the standardized power maps. We performed the split-cohort analysis by dividing subjects into even and odd subgroups, calculating the standardized power maps for both subgroups, and correlating those maps ROI to ROI across the two groups with Pearson's correlations.

The dominant frequency of an area is then simply defined as the band (among all 8) with the largest z score. To test for a robust frequency bias effect in each ROI, where the null hypothesis is that no difference exists between standardized power in each band, we tested for a difference in standardized power using a one-way repeated-measures ANOVA (148 tests) and used the FDR (Genovese et al. 2002) to correct for multiple comparisons. If the ANOVA was significant in a particular ROI, we then tested if the standardized power of the dominant frequency was greater than that in the remaining seven bands via paired one-sided t-tests (7 tests per ROI) and corrected for all tests again using FDR ($q = 0.05$). For ROIs that passed all seven tests, this area was considered to have a strong frequency or timescale bias. For regions where the ANOVA was significant but fewer than seven post hoc t-tests were passed, this region was considered to have a weak bias. Although the Lilliefors test suggests that the vast majority of distributions were normal, the analyses were also repeated with the associated nonparametric tests (Friedman and Wilcoxon signed-rank tests) and also FDR corrected. All analyses were implemented in MATLAB using built-in functions and custom code.

MEG cluster analysis. Because many regions did not have a strong frequency bias, we performed a data-driven analysis of the spectrum to identify if multiple frequency bands might be more consistently dominant together and if these formed canonical spectral profiles across the cortex. To examine the number of distinct canonical spectral profiles across the cortex and how regions grouped by those profiles, we used K-means cluster analysis to cluster regions based on the standardized power in the eight frequency bands. Because we wanted to examine how reliable ROI cluster assignments were across subjects, we used all subjects' ROIs (30 subjects × 148 ROIs = 4,440 total ROI patterns) as observations and their standardized power measurements (8 bands) as dimensions or features. For each ROI, the overall cluster membership was assigned on the basis of plurality vote [the cluster with the most subjects choosing it, which is not necessarily the majority (>15/30 in this study), especially in cases where $k > 2$ clusters). Clustering results were examined for $k = 2$ through

$k = 10$ clusters. Several measures were then examined to pick a k that best captured the cortical frequency organization. First, the variance explained was examined for each k by calculating the total sum of squares minus the within-cluster sum of squares and dividing by the total sum of squares for a percentage measure. Also, the reliability of a particular ROI being assigned the same cluster across subjects was assessed using nonparametric statistics. Control distributions were constructed by first randomly assigning an ROI for each subject to a cluster (out of k) and summing the number of subjects with each cluster assignment. We repeated this process 10,000 times to build a null distribution for each choice of k. We then compared the number of subjects matching the actual plurality cluster assignment with the null distribution to calculate the probability that this number was significantly greater than the null values (with $\alpha < 0.05$). Finally, using the derived P values, we performed FDR correction ($q = 0.05$) over the 148 ROI tests. This nonparametric approach was used for each choice of k, and the number of ROIs failing to survive FDR correction were tabulated. Similarity matrices were calculated for each cluster to examine the strength and uniqueness of cluster membership for a given ROI. Finally, multidimensional scaling was also used to assess the cluster groupings of ROIs in a more visually appropriate two-dimensional (rather than 8-dimensional) plot. The K-means algorithm was performed many times for each k (at least 10 times) with many random starting cluster assignments to assess stability (i.e., are the same clustering results returned each time?), and the results were highly consistent across each repetition. All analyses were implemented in MATLAB using built-in functions and custom code.

RESULTS

To address our first question—Does the hierarchical organization of timescales hold if we examine the whole cortex in humans?—we compared measures of source-localized, standardized power (see MATERIALS AND METHODS for details) from spontaneous MEG data across eight frequency bands in each region of the Destrieux parcellation to find the timescale bias of each region. Cortical standardized power maps are shown as pial maps in Fig. 1 for each frequency band with each map scaled to the maximum and minimum z scores of that band to illustrate their cortical locations. Although the three gamma bands appear very similar and are illustrated separately in Fig. 1, statistical tests presented below demonstrate some differentiation between them. For each frequency band, clear regional differences in standardized power appeared across the cortex. Delta power (0.5–4 Hz) peaks in medial frontal regions and is very strong in lateral frontal, insular, and primary auditory (transverse temporal gyrus/sulcus) regions. Theta (4–8 Hz) has a similar regional profile but is weaker in insula and the transverse temporal cortex. Alpha (8–14 Hz) is strongest in occipital and parietal regions. Low beta (14–20 Hz) is stronger over sensorimotor and parietal cortex, whereas high beta (20–30 Hz) is stronger in sensorimotor and frontal cortex. Standardized power in the three gamma bands (low gamma, 30–50 Hz; high gamma 1, 50–100 Hz; high gamma 2, 100–150 Hz) is strongest in ventral and lateral temporal and frontal regions.

We also calculated the interindividual variability by calculating the standard deviation of the standardized power maps. This is shown in Fig. 2 as standard deviation of the z scores, and generally most regions have low variability, suggesting that the standardized power maps are fairly consistent across individual subjects. Interestingly, parts of the visual and inferior temporal cortex show greater variability in several bands. We also performed a split-cohort analysis by dividing subjects into even and odd subgroups, calculating the standardized power maps for both subgroups, and correlating those maps ROI to ROI across the two groups. The Pearson's correlation coefficient was consistently very high across all bands (0.93 for delta, 0.98 for theta, 0.99 for alpha, 0.96 for low beta, 0.96 for high beta, 0.93 for low gamma, 0.96 for high gamma 1, 0.97 for high gamma 2), suggesting these maps are highly reliable.

Next, for each ROI, the frequency band with the greatest standardized power (max power) was determined and compared with the standardized power in the remaining seven bands to examine frequency biases. In all ROIs the dominant frequency was significantly greater than at least one other frequency (ANOVA, $P < 0.05$, FDR corrected for 148 tests), suggesting that in no region was standardized spectral power flat. Of 148 ROIs, 67 displayed a strong frequency bias where all 7 post hoc tests were significant (paired, 1-sided t-test, $P < 0.05$, FDR corrected for $148 \times 7 = 1{,}036$ tests). These regions and their respective dominant frequencies are displayed in Fig. 3*A* (see color legend at *left* for frequency bias of a region). Most frequency bands were well represented in the dominant frequencies, but this map does not obviously relate to a sensory-to-higher order hierarchical scheme. For example, higher frequencies such as high beta and high gamma 2 are in higher order areas such as lateral frontal and superior/inferior temporal gyrus, respectively, and delta power is dominant in the transverse temporal cortex, a primary sensory region. Note that the ANOVA results presented in Fig. 3*A* demonstrate some statistical differentiation between the gamma bands, i.e., one of the three gamma bands is strongly biased over the others in some frontal and temporal regions. For each ROI, the number of t-tests passed was summed, and a histogram (Fig. 3*C*) demonstrates that a slight majority of regions did not have a strong bias; in fact, many regions had two to three frequencies that were not significantly different in standardized power. Because the dominant frequency was significantly greater than at least one other frequency in all ROIs, all regions may have at least a weak bias (Fig. 3*B*). Results from associated nonparametric tests were nearly identical to the results from parametric tests. Only the right and left temporal pole differed between the strong bias results, with high gamma 2 appearing in the right rather than the left pole, and the weak bias results are identical. Thus the parametric and nonparametric results converge well, and we have displayed only the parametric results for simplicity.

Given that the timescale to region relationship was not robustly hierarchical or even corresponding in a one-to-one manner, we used K-means cluster analysis, a data-driven approach, to examine the relationship between rhythmic neural activity and cortical region in an unbiased manner. Because a slight majority of regions did not display a strong bias toward one particular frequency band, we expected that the spectral profile of a region would show strong standardized power in multiple bands in some cases. The clustering analysis, performed on spectral dimensions of all subjects' ROIs (i.e., 8 frequency band dimensions and $30 \times 148 = 4{,}440$ total ROIs) indeed demonstrated the grouping of specific frequency bands for some profiles. For the group maps in Fig. 4, the cluster to which each ROI was assigned was chosen on the basis of the most common cluster assignment across all subjects' ROIs. To determine how many spectral profiles or clusters existed in the

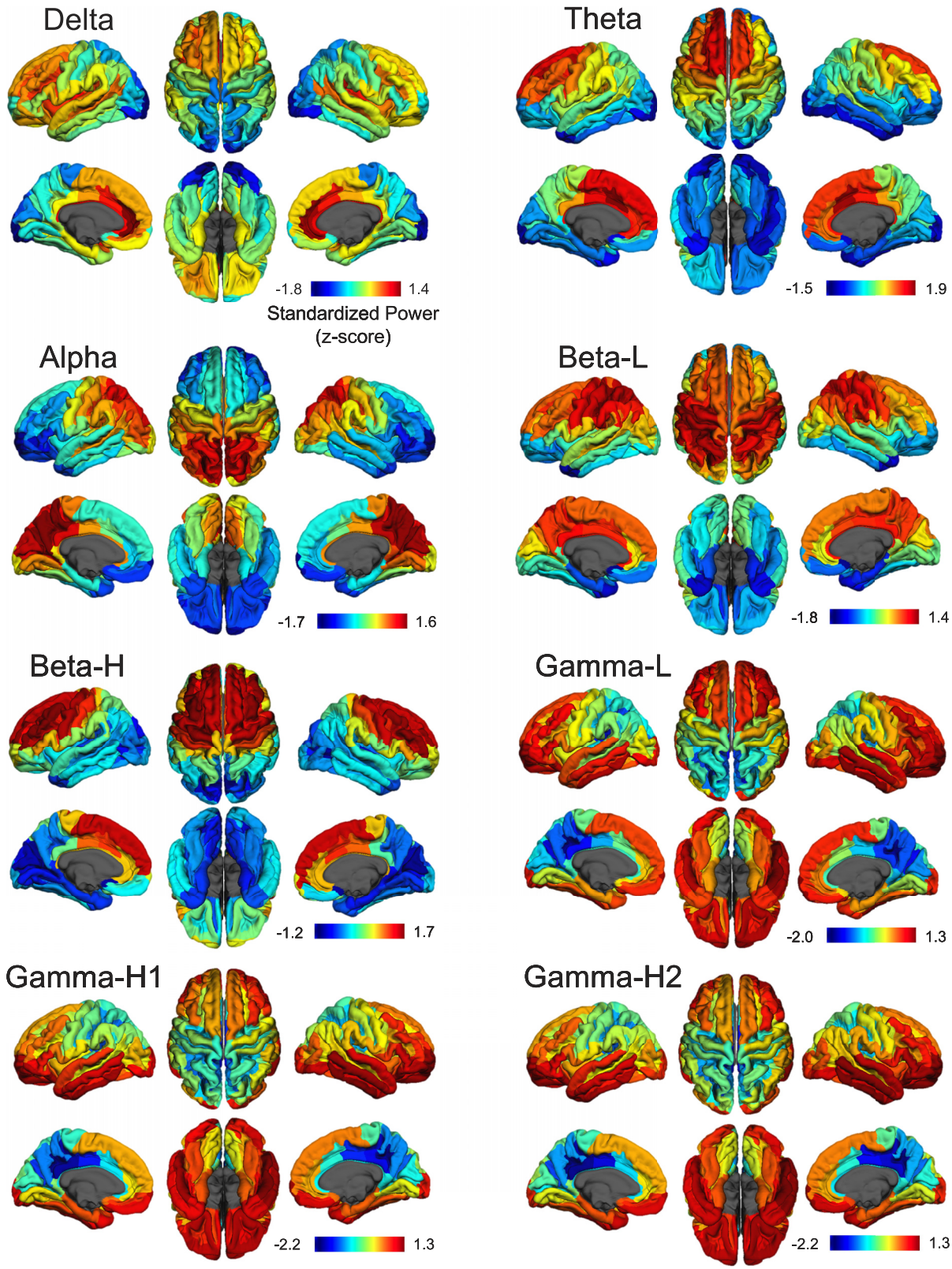

Fig. 1. Standardized power maps for each frequency band. Spectral power was standardized from spatial measures of power separately for each band, effectively creating minimal-maximal (min-max) maps in units of standard deviation; therefore, color bars are in units of z scores and do not correspond across frequency bands so that locations of max and min can be shown separately for each band. Bands are divided into delta (0.5–4 Hz), theta (4–8 Hz), alpha (8–14 Hz), beta low (beta-L; 14–20 Hz), beta high (beta-H; 20–30 Hz), low gamma (gamma-L; 30–50 Hz), high gamma 1 (gamma-H1; 50–100 Hz), and high gamma 2 (gamma-H2; 100–150 Hz) and are shown by Destrieux atlas ROIs on pial surface maps of the fsaverage brain.

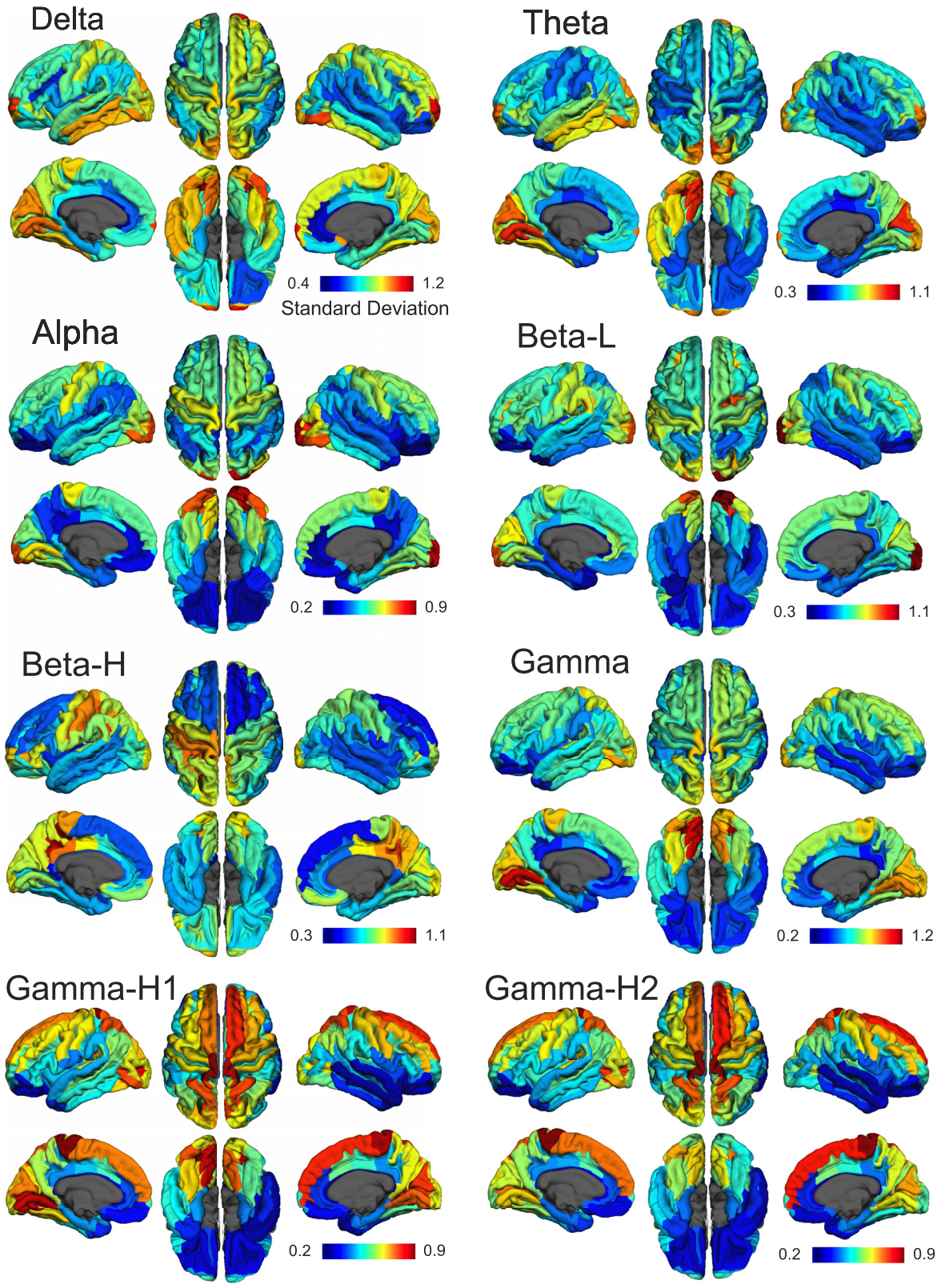

Fig. 2. Interindividual variability maps. Interindividual variability of standardized power is demonstrated through the standard deviation of z scores across subjects for each frequency band. Maps for each band are scaled separately to the max and min standard deviations.

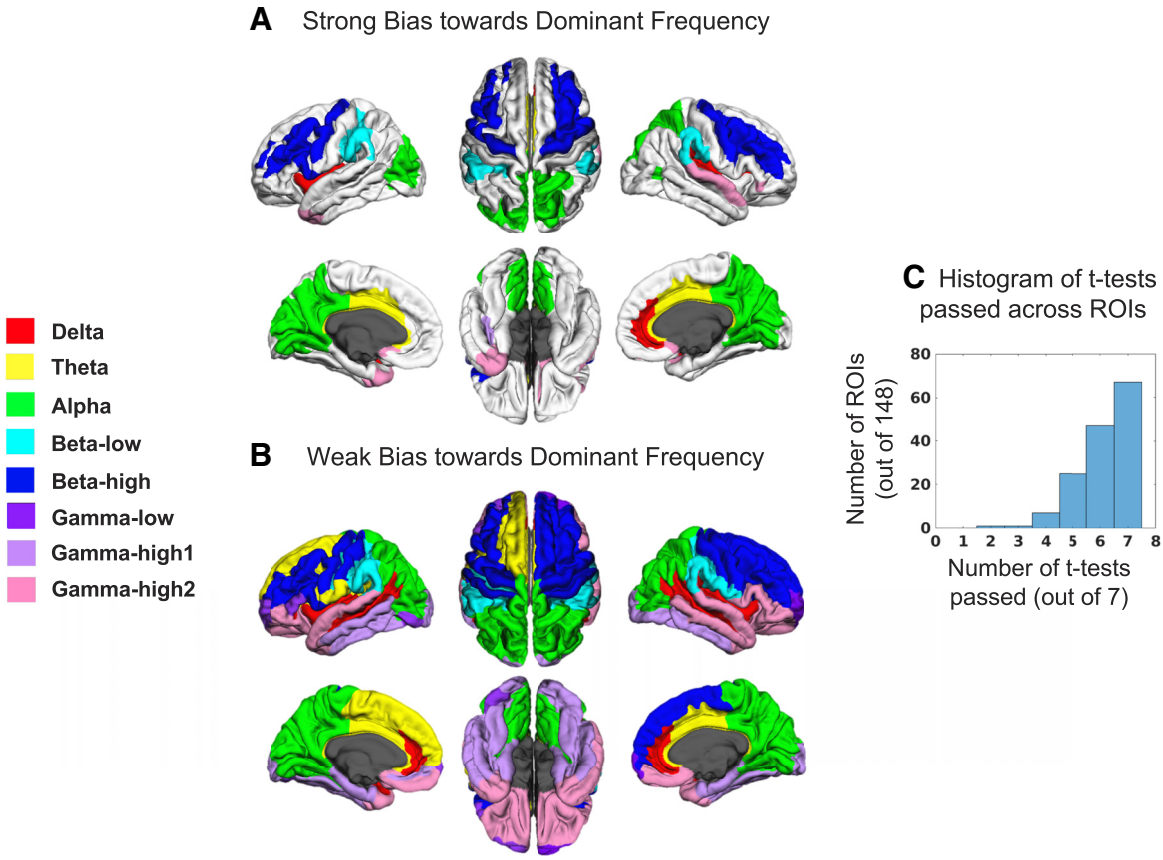

Fig. 3. Dominant frequency maps. *A*: cortical regions showing a strong bias (defined as a frequency with maximal standardized power > standardized power of all other frequencies, $P < 0.05$, FDR corrected) toward the dominant frequency. Dominant frequency for an ROI is color coded according to the legend at *left*. *B*: cortical regions showing a weak bias (frequency with maximal standardized power > standardized power of at least one other frequency, $P < 0.05$, FDR corrected) toward the dominant frequency. *C*: for each ROI, 7 post hoc paired, one-sided *t*-tests were performed to compare frequencies. The histogram shows the number of ROIs passing the stated number of *t*-tests. Only about half of the ROIs show a strong bias (all 7 tests passed at $\alpha < 0.05$, FDR corrected), suggesting many regions do not have strong timescale biases.

data, results for $k = 2$ through 10 clusters were examined to find the optimal model reliability and complexity trade-offs. The variance in power explained by number of clusters (i.e., total sum of squares minus within-cluster sum of squares, divided by total sum of squares for percentage; Fig. 4*A*) showed a gradual increase with number of clusters, but $k = 3$ was the first to explain >50% variance. Nonparametric permutation tests were used to examine cross-subject clustering reliability and assist in choosing k by comparing actual cluster assignments with random cluster assignment of subjects' ROIs (see MATERIALS AND METHODS for full details of nonparametric testing). They revealed that increasing k decreased the number of ROIs failing to reach significance (those $P > 0.05$ after FDR correction), i.e., ROIs inconsistently clustered across subjects (Fig. 4*B*, blue line). There was a trade-off, however, with the number of ROIs being assigned clusters on the basis of a plurality (largest subset of subjects) but not a majority (more than half of the subjects) vote among all subjects (Fig. 4*B*, green line). Ideally, cluster assignments based on a majority would be better, and this argued for use of a smaller k. Based on these findings, results from $k = 3$, 4, and 5 clusters were all deemed optimal. Figure 4*C* displays the results for $k = 3$ clusters, where the three spectral profiles (second column) one with an alpha peak, one with delta, theta, low-beta, and high-beta peaks, and one with a peak across the gamma bands, are quite distinct and spatially localized to visual and parietal cortices, dorsal frontal cortex, and temporal and ventral frontal cortex (first row), respectively. The similarity matrix (third column) and multidimensional scaling (MDS) plot (fourth column) also show good agreement with the K-means cluster assignments, demonstrating consistent results across distinct methods. For $k = 4$ clusters (Fig. 4*D*), an additional profile displays peaks in delta and gamma bands and is located in lateral and ventral temporal and frontal regions. For $k = 5$ clusters (Fig. 4*E*), an additional profile exists, peaking in alpha but not as low in gamma (gold line), and is distinct from another profile (green line), which is high in alpha power but much lower in gamma power. This profile is preferred in some regions of visual and inferior parietal cortices. Similarity matrices and MDS plots for $k = 4$ and 5 also show good agreement across methods. White ROIs on cortical surface maps did not pass the nonparametric permutation test after FDR correction for multiple comparisons ($P > 0.05$), indicating that they were inconsistently clustered across subjects. All colored ROIs did pass the FDR-corrected tests ($P < 0.05$).

DISCUSSION

In this study, we examined if the proposed hierarchical relationship between timescales of intrinsic rhythmic activity and anatomical region found in monkeys (Murray et al.

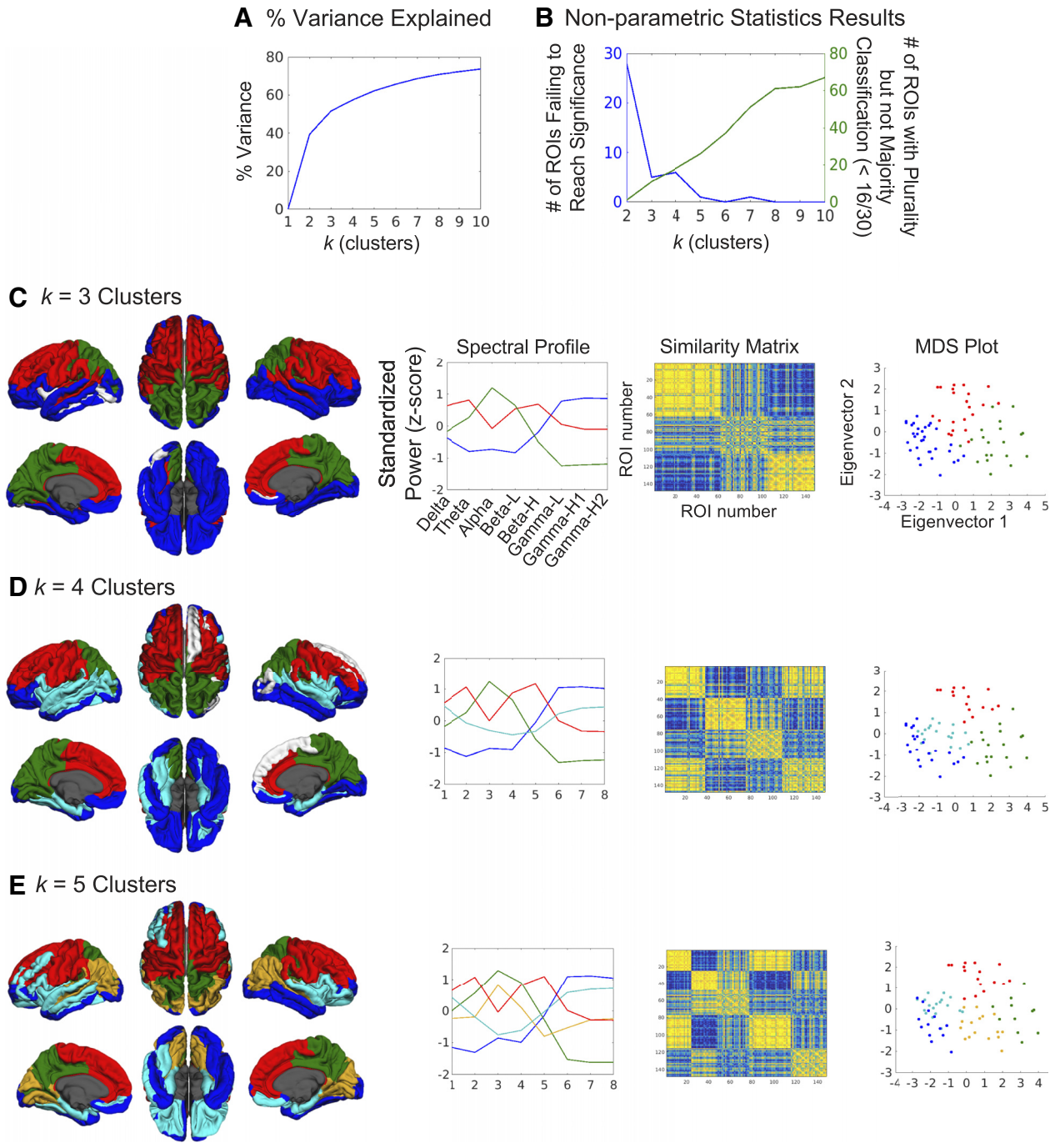

Fig. 4. Clustering reveals several spectral profiles across the cortex. *A*: ROIs were clustered by spectral features using K-means analysis for $k = 2$ through 10 clusters. The percent variance explained by each cluster solution is graphed. *B*: nonparametric statistics demonstrated clustering consistency across subjects (i.e., whether each ROI consistently assigned the same cluster spectral profile across all subjects). The blue line in the graph plots the number of ROIs that were not consistently clustered for each solution of k. The green line plots the number of ROIs that were consistently clustered across subjects but have a plurality (largest subset), not a majority, of subjects picking the same spectral profile for a given ROI. As k increases, the number of possible clusters assigned to an ROI increases, making it harder to achieve a majority of at least 16/30 subjects. Both graphs helped us determine that $k = 3$, 4, and 5 were solutions fitting a good trade-off of model reliability and complexity. *C*: cortical maps of the $k = 3$ cluster solution (first column) where colors index the spectral profiles (second column). White ROIs on cortical surface maps did not pass the permutation test after FDR correction. The similarity matrix (third column) shows reasonably tight clustering across the 3 clusters. The multidimensional scaling (MDS) plot of ROIs (fourth column) also demonstrates tight clustering with this solution. *D*: the $k = 4$ cluster solution. *E*: the $k = 5$ cluster solution.

2014) holds in humans across the whole cortex, especially when power measures across a wider spectrum of neurophysiological frequencies are taken into account. We did not find a robust sensory-to-higher order hierarchical relationship, suggesting that the relationship between the frequency of rhythmic activity (and their corresponding timescales) and cortical region may be more complex. Subsequent novel data-driven analysis instead revealed that in many regions of cortex, multiple timescales across the spectrum predominate.

In pursuing novel characterization of broader spectral profiles and their similarities across cortex to answer the hierarchy question, we were able to replicate and expand on previous reports of localized power in the literature. Although EEG/MEG sources are still rarely estimated, our results show that the standardized power peaks in specific bands correspond well with previous reports of both task-dependent and spontaneous raw power. Delta power has previously been correlated with PET metabolism in medial frontal regions (Alper et al. 2006), whereas localized frontal-midline theta power concentrates in the anterior cingulate cortex (Ishii et al. 1999; Mitchell et al. 2008). Based on modulation during eyes-open and -closed paradigms, alpha has long been thought to index visual processing and has been localized to both ventral and dorsal visual regions (Capilla et al. 2014; Hari and Salmelin 1997; Salmelin and Hari 1994; Tuladhar et al. 2007). Reactivity in the beta band is often tied to motor movement and somatosensory stimulation (Neuper et al. 2006) and has been localized to somatosensory, motor, and frontal cortices (Baumgartner et al. 1991; Salenius et al. 1997; Sherman et al. 2016). Finally, because different sub-bands within the whole gamma band have been observed across the cortex during different tasks and may index different processes (Crone et al. 2011), we did not expect to see peaks in any particular region for gamma power. Still, the distribution across inferior temporal and frontal regions has been observed with spontaneous ECoG recordings (Groppe et al. 2013).

Also, although it is only one step toward addressing the study's questions, we present one of the first approaches to create comprehensive, source-localized spectral maps for 0.5–150 Hz. Our approach confirms and builds on findings from two recent studies that created whole cortex frequency maps up to 48 or 120 Hz (see supplementary materials, respectively, of Hillebrand et al. 2016 and Keitel and Gross 2016). Our results are remarkably similar to the topographies of each band reported by Hillebrand et al. (2016), except for a gamma-band discrepancy where they only found frontal peaks. Our results are also similar to the report by Keitel and Gross (2016), including elevated gamma power in inferior temporal and frontal regions, and their analysis focuses on the different spectral modes in which an ROI may operate. Interestingly, different source-localization algorithms were used across the three studies (beamforming vs. MNE), but this made little difference between the main results. Another powerful approach of correlating power in each band with functional MRI BOLD resting-state networks has also revealed reactivity of multiple frequency bands within each network (Liu et al. 2014; Mantini et al. 2007), with alpha peaking in the visual network, beta in somatomotor, delta (and sometimes theta and beta) in auditory, and gamma in frontal regions. When specific cortical regions are stimulated with transcranial magnetic stimulation (TMS), the resonant frequencies of the ensuing oscillations are also region specific: alpha in occipital, beta in parietal, and beta-gamma in frontal regions (Rosanova et al. 2009). The reproducibility of the spatial selectivity of these frequencies across multiple methods further supports the robustness of these findings and our novel approach to measuring and extending them.

Although they are useful to compare localization results with other findings, these other studies did not directly address the question of whether the timescales of different bands correlated with a sensory-to-higher order processing hierarchy. Even if we roughly define sensory regions as lower order processing areas and association cortices as higher order processing areas, we *1*) do not find strong biases toward particular timescales across all cortical regions and *2*) do not exclusively find that lower areas are biased to faster frequencies and higher areas are biased to slower frequencies as predicted from the monkey data. For example, delta power (timescales of ~250–1,000 ms) is dominant on the transverse temporal cortex where early sensory, lower order auditory processing occurs, and beta and gamma power (timescales of ~10–50 ms) are dominant in much of frontal cortex involved in higher level cognition. Additionally, the clustering analysis shows that rhythmic activity occurring at multiple timescales is widespread, with higher theta and gamma activity in dorsal frontal regions and higher delta and gamma activity in temporal and ventral frontal regions.

Ultimately, a major goal is to elucidate the functions of this rhythmic neural activity. Examining them in the context of tasks has been very fruitful, but recent approaches have been finding that examining rhythmic oscillations with regard to spatial organization may also help. Recent studies have focused on the role of these oscillations in feedforward and feedback processing. In monkeys, studies have found that gamma synchronization is biased toward superficial layers and alpha-beta toward infragranular layers of visual cortex (Buffalo et al. 2011; van Kerkoerle et al. 2014; Xing et al. 2012). Directed connectivity measures have shown that in the human visual system, higher frequencies (gamma) may carry information forward and lower frequencies (alpha, beta) carry it back to lower order regions (Michalareas et al. 2016), whereas in the human auditory system, gamma carries information forward and delta-beta carries it back (Fontolan et al. 2014). Thus frequency bands may serve as channels of communication across layers and regions (see also Hillebrand et al. 2016), but, crucially, this depends on activity operating in multiple bands within each region. More recently, it has been proposed that the ventral visual pathway is best thought of as containing recurrent occipitotemporal networks in contrast to a predominantly serial hierarchy (Kravitz et al. 2013). Along with the oscillatory feedforward/feedback mechanisms, these data also suggest that an architecture where sensory regions only operate at faster timescales and higher order areas at slower timescales to integrate information over time (Honey et al. 2012) may be too simplistic; perhaps it is the interactions between sensory and high-order areas at faster or slower timescales that support accumulating information.

A beneficial output from this study may also be the realization that examining standardized power (assuming sufficient sampling of power across the cortex) may be a useful approach to comparing across frequency bands in future studies of normal and patient brains. As pointed out before (Mantini et al. 2007), examining the whole spectrum gives a more complete, less biased view of neural processing than examining individual bands. However, it has not always been clear how to compare across the bands given the 1/*f* power drop-off, and this is one way to move beyond that limitation (see Groppe et al. 2013 and Keitel and Gross 2016 for other approaches).

Some caveats exist with this analysis, however. First, gamma-band activity suffers from low signal-to-noise ratio due to the 1/*f* power drop-off in the brain and can be dominated by

muscular artifacts. Although we took care to exclude as many artifacts from the data as possible (eyeblinks and saccades via ICA and jaw movements via sensoring of data with large-amplitude gamma) and confirmed no associations between ocular muscle activity and the gamma bands, the gamma activity should still be interpreted with caution. A recent review of this issue (Muthukumaraswamy 2013) reported no guaranteed ways to remove all possible gamma artifacts but suggested that after care is taken to remove them through known methods, as we did, there is still value in examining the gamma band. Second, this is an amplitude-centric analysis because the frequency bias measures are based on relative power. Many studies have demonstrated that the phase of rhythmic activity plays a unique and important role in neural processing and modulation, as well as perception and cognition (Busch et al. 2009; Mathewson et al. 2009; Roux et al. 2013), but phase has not been considered in this study. An analysis that examines that feature could provide a more fine-grained organization of cortical oscillations and answer how phase varies across large areas oscillating at a particular frequency (e.g., is there an alpha phase gradient between occipital and parietal cortex akin to traveling waves?; Maris et al. 2016). However, phase likely changes relative to the start of a resting-state MEG scan, so phase relative to other rhythms across cortex, i.e., connectivity analysis, may be a another approach to understanding variations in phase (see Kida et al. 2016 for a review of phase as an important component of many types of connectivity analysis). Additionally, we have only examined the intrinsic organization, so a task-based organization may differ depending on the task requirements. For example, alpha activity is also modulated in other sensory regions for modality-specific spatial attention (Haegens et al. 2011; Müller and Weisz 2012), so the frequencies in these maps are not the only operating modes for a particular region. Even in early visual cortex, changes between spontaneous and naturalistic stimulation are seen throughout the spectrum (Sellers et al. 2015). Investigating how intrinsic and task-related organizations are related, as well as whether they support or influence each other, is an important avenue of research (Ghuman et al. 2013; Keitel and Gross 2016; Lewis et al. 2016). Finally, the intrinsic frequency organization may also change with time given that the processes generating it are possibly nonstationary, but this was not considered in this time-independent analysis because it did not help address the hierarchy question. Keitel and Gross (2016) have found similar spectral profiles to those presented in this article by using a time-varying multitaper analysis, but their results suggest that a region can take on multiple spectral modes that may be superimposed in our maps. As an example, the spectral profile with high delta, theta, and beta power in frontal regions may reflect two modes of operation: one peaking in delta-theta and one peaking in beta. Still, the methodology of nonstationary analysis must be executed and results interpreted carefully because stationary data can be incorrectly found to be nonstationary (e.g., Hlinka and Hadrava 2015; Laumann et al. 2017).

In conclusion, we have found a complex organization between frequency and cortical region across the human brain that does not follow a sensory-to-higher order hierarchy. More work remains to elucidate the origins of this organization and its functional utility.

GRANTS

This work was supported by the Intramural Research Program of the National Institute of Mental Health, National Institutes of Health, and it was conducted under NIH Clinical Study Protocol 93-M-0170 (ZIAMH002588); NCT00001360.

DISCLOSURES

No conflicts of interest, financial or otherwise, are declared by the authors.

AUTHOR CONTRIBUTIONS

M.S.M. and A.M. conceived and designed research; M.S.M., S.W., and S.J.G. analyzed data; M.S.M., S.J.G., A.S.G., and A.M. interpreted results of experiments; M.S.M. prepared figures; M.S.M. and S.W. drafted manuscript; M.S.M., S.W., S.J.G., A.S.G., and A.M. edited and revised manuscript; M.S.M., S.W., S.J.G., A.S.G., and A.M. approved final version of manuscript; A.S.G. performed experiments.

REFERENCES

Alper KR, John ER, Brodie J, Günther W, Daruwala R, Prichep LS. Correlation of PET and qEEG in normal subjects. *Psychiatry Res* 146: 271–282, 2006. doi:10.1016/j.pscychresns.2005.06.008.

Baumgartner C, Barth DS, Levesque MF, Sutherling WW. Functional anatomy of human hand sensorimotor cortex from spatiotemporal analysis of electrocorticography. *Electroencephalogr Clin Neurophysiol* 78: 56–65, 1991. doi:10.1016/0013-4694(91)90019-Z.

Buffalo EA, Fries P, Landman R, Buschman TJ, Desimone R. Laminar differences in gamma and alpha coherence in the ventral stream. *Proc Natl Acad Sci USA* 108: 11262–11267, 2011. doi:10.1073/pnas.1011284108.

Busch NA, Dubois J, VanRullen R. The phase of ongoing EEG oscillations predicts visual perception. *J Neurosci* 29: 7869–7876, 2009. doi:10.1523/JNEUROSCI.0113-09.2009.

Buzsáki G. *Rhythms of the Brain*. New York: Oxford University Press, 2006.

Capilla A, Schoffelen J-M, Paterson G, Thut G, Gross J. Dissociated α-band modulations in the dorsal and ventral visual pathways in visuospatial attention and perception. *Cereb Cortex* 24: 550–561, 2014. doi:10.1093/cercor/bhs343.

Crone NE, Korzeniewska A, Franaszczuk PJ. Cortical γ responses: searching high and low. *Int J Psychophysiol* 79: 9–15, 2011. doi:10.1016/j.ijpsycho.2010.10.013.

Destrieux C, Fischl B, Dale A, Halgren E. Automatic parcellation of human cortical gyri and sulci using standard anatomical nomenclature. *Neuroimage* 53: 1–15, 2010. doi:10.1016/j.neuroimage.2010.06.010.

Eggermont JJ, Tass PA. Maladaptive neural synchrony in tinnitus: origin and restoration. *Front Neurol* 6: 29, 2015. doi:10.3389/fneur.2015.00029.

Engel AK, Fries P, Singer W. Dynamic predictions: oscillations and synchrony in top-down processing. *Nat Rev Neurosci* 2: 704–716, 2001. doi:10.1038/35094565.

Fontolan L, Morillon B, Liegeois-Chauvel C, Giraud AL. The contribution of frequency-specific activity to hierarchical information processing in the human auditory cortex. *Nat Commun* 5: 4694, 2014. doi:10.1038/ncomms5694.

Fries P. Rhythms for cognition: communication through coherence. *Neuron* 88: 220–235, 2015. doi:10.1016/j.neuron.2015.09.034.

Gauthier B, Eger E, Hesselmann G, Giraud AL, Kleinschmidt A. Temporal tuning properties along the human ventral visual stream. *J Neurosci* 32: 14433–14441, 2012. doi:10.1523/JNEUROSCI.2467-12.2012.

Genovese CR, Lazar NA, Nichols T. Thresholding of statistical maps in functional neuroimaging using the false discovery rate. *Neuroimage* 15: 870–878, 2002. doi:10.1006/nimg.2001.1037.

Ghuman AS, McDaniel JR, Martin A. A wavelet-based method for measuring the oscillatory dynamics of resting-state functional connectivity in MEG. *Neuroimage* 56: 69–77, 2011. doi:10.1016/j.neuroimage.2011.01.046.

Ghuman AS, van den Honert RN, Martin A. Interregional neural synchrony has similar dynamics during spontaneous and stimulus-driven states. *Sci Rep* 3: 1481, 2013. doi:10.1038/srep01481.

Gramfort A, Luessi M, Larson E, Engemann DA, Strohmeier D, Brodbeck C, Parkkonen L, Hämäläinen MS. MNE software for processing MEG and EEG data. *Neuroimage* 86: 446–460, 2014. doi:10.1016/j.neuroimage.2013.10.027.

Groppe DM, Bickel S, Keller CJ, Jain SK, Hwang ST, Harden C, Mehta AD. Dominant frequencies of resting human brain activity as measured by

the electrocorticogram. *Neuroimage* 79: 223–233, 2013. doi:10.1016/j.neuroimage.2013.04.044.

Haegens S, Händel BF, Jensen O. Top-down controlled alpha band activity in somatosensory areas determines behavioral performance in a discrimination task. *J Neurosci* 31: 5197–5204, 2011. doi:10.1523/JNEUROSCI.5199-10.2011.

Hämäläinen M. *MNE Software User's Guide, Version 2.7*, 2009. https://pdfs.semanticscholar.org/d7e0/2809ac388578595d612f8f989326368ee697.pdf.

Hämäläinen MS, Ilmoniemi RJ. Interpreting magnetic fields of the brain: minimum norm estimates. *Med Biol Eng Comput* 32: 35–42, 1994. doi:10.1007/BF02512476.

Hämäläinen MS, Sarvas J. Realistic conductivity geometry model of the human head for interpretation of neuromagnetic data. *IEEE Trans Biomed Eng* 36: 165–171, 1989. doi:10.1109/10.16463.

Hansen P, Kringelbach M, Salmelin R (editors). *MEG: An Introduction to Methods*. New York: Oxford University Press, 2010, p. 201.

Hari R, Puce A. *MEG-EEG Primer*. New York: Oxford University Press, 2017, p. 83.

Hari R, Salmelin R. Human cortical oscillations: a neuromagnetic view through the skull. *Trends Neurosci* 20: 44–49, 1997. doi:10.1016/S0166-2236(96)10065-5.

Hasson U, Chen J, Honey CJ. Hierarchical process memory: memory as an integral component of information processing. *Trends Cogn Sci* 19: 304–313, 2015. doi:10.1016/j.tics.2015.04.006.

He BJ, Snyder AZ, Zempel JM, Smyth MD, Raichle ME. Electrophysiological correlates of the brain's intrinsic large-scale functional architecture. *Proc Natl Acad Sci USA* 105: 16039–16044, 2008. doi:10.1073/pnas.0807010105.

Heusser AC, Poeppel D, Ezzyat Y, Davachi L. Episodic sequence memory is supported by a theta-gamma phase code. *Nat Neurosci* 19: 1374–1380, 2016. doi:10.1038/nn.4374.

Hillebrand A, Tewarie P, van Dellen E, Yu M, Carbo EW, Douw L, Gouw AA, van Straaten EC, Stam CJ. Direction of information flow in large-scale resting-state networks is frequency-dependent. *Proc Natl Acad Sci USA* 113: 3867–3872, 2016. doi:10.1073/pnas.1515657113.

Hlinka J, Hadrava M. On the danger of detecting network states in white noise. *Front Comput Neurosci* 9: 11, 2015. doi:10.3389/fncom.2015.00011.

Honey CJ, Thesen T, Donner TH, Silbert LJ, Carlson CE, Devinsky O, Doyle WK, Rubin N, Heeger DJ, Hasson U. Slow cortical dynamics and the accumulation of information over long timescales. *Neuron* 76: 423–434, 2012. doi:10.1016/j.neuron.2012.08.011.

Ishii R, Shinosaki K, Ukai S, Inouye T, Ishihara T, Yoshimine T, Hirabuki N, Asada H, Kihara T, Robinson SE, Takeda M. Medial prefrontal cortex generates frontal midline theta rhythm. *Neuroreport* 10: 675–679, 1999. doi:10.1097/00001756-199903170-00003.

Jung TP, Makeig S, Humphries C, Lee TW, McKeown MJ, Iragui V, Sejnowski TJ. Removing electroencephalographic artifacts by blind source separation. *Psychophysiology* 37: 163–178, 2000. doi:10.1111/1469-8986.3720163.

Keitel A, Gross J. Individual human brain areas can be identified from their characteristic spectral activation fingerprints. *PLoS Biol* 14: e1002498, 2016. doi:10.1371/journal.pbio.1002498.

Kida T, Tanaka E, Kakigi R. Multi-dimensional dynamics of human electromagnetic brain activity. *Front Hum Neurosci* 9: 713, 2016. doi:10.3389/fnhum.2015.00713.

Kiebel SJ, Daunizeau J, Friston KJ. A hierarchy of time-scales and the brain. *PLoS Comput Biol* 4: e1000209, 2008. doi:10.1371/journal.pcbi.1000209.

Kravitz DJ, Saleem KS, Baker CI, Ungerleider LG, Mishkin M. The ventral visual pathway: an expanded neural framework for the processing of object quality. *Trends Cogn Sci* 17: 26–49, 2013. doi:10.1016/j.tics.2012.10.011.

Laumann TO, Snyder AZ, Mitra A, Gordon EM, Gratton C, Adeyemo B, Gilmore AW, Nelson SM, Berg JJ, Greene DJ, McCarthy JE, Tagliazucchi E, Laufs H, Schlaggar BL, Dosenbach NU, Petersen SE. On the stability of BOLD fMRI correlations. *Cereb Cortex* 27: 4719–4732, 2017. doi:10.1093/cercor/bhw265.

Lewis CM, Bosman CA, Womelsdorf T, Fries P. Stimulus-induced visual cortical networks are recapitulated by spontaneous local and interareal synchronization. *Proc Natl Acad Sci USA* 113: E606–E615, 2016. doi:10.1073/pnas.1513773113.

Lin FH, Witzel T, Hämäläinen MS, Dale AM, Belliveau JW, Stufflebeam SM. Spectral spatiotemporal imaging of cortical oscillations and interactions in the human brain. *Neuroimage* 23: 582–595, 2004. doi:10.1016/j.neuroimage.2004.04.027.

Liu Z, de Zwart JA, Chang C, Duan Q, van Gelderen P, Duyn JH. Neuroelectrical decomposition of spontaneous brain activity measured with functional magnetic resonance imaging. *Cereb Cortex* 24: 3080–3089, 2014. doi:10.1093/cercor/bht164.

Lozano-Soldevilla D, ter Huurne N, Cools R, Jensen O. GABAergic modulation of visual gamma and alpha oscillations and its consequences for working memory performance. *Curr Biol* 24: 2878–2887, 2014. doi:10.1016/j.cub.2014.10.017.

Mantini D, Perrucci MG, Del Gratta C, Romani GL, Corbetta M. Electrophysiological signatures of resting state networks in the human brain. *Proc Natl Acad Sci USA* 104: 13170–13175, 2007. doi:10.1073/pnas.0700668104.

Maris E, Fries P, van Ede F. Diverse phase relations among neuronal rhythms and their potential function. *Trends Neurosci* 39: 86–99, 2016. doi:10.1016/j.tins.2015.12.004.

Mathewson KE, Gratton G, Fabiani M, Beck DM, Ro T. To see or not to see: prestimulus α phase predicts visual awareness. *J Neurosci* 29: 2725–2732, 2009. doi:10.1523/JNEUROSCI.3963-08.2009.

Michalareas G, Vezoli J, van Pelt S, Schoffelen JM, Kennedy H, Fries P. Alpha-beta and gamma rhythms subserve feedback and feedforward influences among human visual cortical areas. *Neuron* 89: 384–397, 2016. doi:10.1016/j.neuron.2015.12.018.

Mitchell DJ, McNaughton N, Flanagan D, Kirk IJ. Frontal-midline theta from the perspective of hippocampal "theta". *Prog Neurobiol* 86: 156–185, 2008. doi:10.1016/j.pneurobio.2008.09.005.

Müller N, Weisz N. Lateralized auditory cortical alpha band activity and interregional connectivity pattern reflect anticipation of target sounds. *Cereb Cortex* 22: 1604–1613, 2012. doi:10.1093/cercor/bhr232.

Murray JD, Bernacchia A, Freedman DJ, Romo R, Wallis JD, Cai X, Padoa-Schioppa C, Pasternak T, Seo H, Lee D, Wang XJ. A hierarchy of intrinsic timescales across primate cortex. *Nat Neurosci* 17: 1661–1663, 2014. doi:10.1038/nn.3862.

Müsch K, Siegel M, Engel AK, Schneider TR. Gamma-band activity reflects attentional guidance by facial expression. *Neuroimage* 146: 1142–1148, 2017. doi:10.1016/j.neuroimage.2016.09.025.

Muthukumaraswamy SD. High-frequency brain activity and muscle artifacts in MEG/EEG: a review and recommendations. *Front Hum Neurosci* 7: 138, 2013. doi:10.3389/fnhum.2013.00138.

Neuper C, Wörtz M, Pfurtscheller G. ERD/ERS patterns reflecting sensorimotor activation and deactivation. *Prog Brain Res* 159: 211–222,2006.

Oostenveld R, Fries P, Maris E, Schoffelen JM. FieldTrip: Open source software for advanced analysis of MEG, EEG, and invasive electrophysiological data. *Comput Intell Neurosci* 2011: 156869, 2011. doi:10.1155/2011/156869.

Oswal A, Beudel M, Zrinzo L, Limousin P, Hariz M, Foltynie T, Litvak V, Brown P. Deep brain stimulation modulates synchrony within spatially and spectrally distinct resting state networks in Parkinson's disease. *Brain* 139: 1482–1496, 2016. doi:10.1093/brain/aww048.

Palva S, Palva JM. Functional roles of alpha-band phase synchronization in local and large-scale cortical networks. *Front Psychol* 2: 204, 2011. doi:10.3389/fpsyg.2011.00204.

Rosanova M, Casali A, Bellina V, Resta F, Mariotti M, Massimini M. Natural frequencies of human corticothalamic circuits. *J Neurosci* 29: 7679–7685, 2009. doi:10.1523/JNEUROSCI.0445-09.2009.

Roux F, Wibral M, Singer W, Aru J, Uhlhaas PJ. The phase of thalamic alpha activity modulates cortical gamma-band activity: evidence from resting-state MEG recordings. *J Neurosci* 33: 17827–17835, 2013. doi:10.1523/JNEUROSCI.5778-12.2013.

Rutter L, Carver FW, Holroyd T, Nadar SR, Mitchell-Francis J, Apud J, Weinberger DR, Coppola R. Magnetoencephalographic gamma power reduction in patients with schizophrenia during resting condition. *Hum Brain Mapp* 30: 3254–3264, 2009. doi:10.1002/hbm.20746.

Salenius S, Schnitzler A, Salmelin R, Jousmäki V, Hari R. Modulation of human cortical rolandic rhythms during natural sensorimotor tasks. *Neuroimage* 5: 221–228, 1997. doi:10.1006/nimg.1997.0261.

Salmelin R, Hari R. Characterization of spontaneous MEG rhythms in healthy adults. *Electroencephalogr Clin Neurophysiol* 91: 237–248, 1994. doi:10.1016/0013-4694(94)90187-2.

Sellers KK, Bennett DV, Fröhlich F. Frequency-band signatures of visual responses to naturalistic input in ferret primary visual cortex during free viewing. *Brain Res* 1598: 31–45, 2015. doi:10.1016/j.brainres.2014.12.016.

Sherman MA, Lee S, Law R, Haegens S, Thorn CA, Hämäläinen MS, Moore CI, Jones SR. Neural mechanisms of transient neocortical beta rhythms: Converging evidence from humans, computational modeling, monkeys, and mice. *Proc Natl Acad Sci USA* 113: E4885–E4894, 2016. doi:10.1073/pnas.1604135113.

Singer W. Cortical dynamics revisited. *Trends Cogn Sci* 17: 616–626, 2013. doi:10.1016/j.tics.2013.09.006.

Tuladhar AM, ter Huurne N, Schoffelen JM, Maris E, Oostenveld R, Jensen O. Parieto-occipital sources account for the increase in alpha activity with working memory load. *Hum Brain Mapp* 28: 785–792, 2007. doi:10.1002/hbm.20306.

Uhlhaas PJ. Dysconnectivity, large-scale networks and neuronal dynamics in schizophrenia. *Curr Opin Neurobiol* 23: 283–290, 2013. doi:10.1016/j.conb.2012.11.004.

van Kerkoerle T, Self MW, Dagnino B, Gariel-Mathis MA, Poort J, van der Togt C, Roelfsema PR. Alpha and gamma oscillations characterize feedback and feedforward processing in monkey visual cortex. *Proc Natl Acad Sci USA* 111: 14332–14341, 2014. doi:10.1073/pnas.1402773111.

Xing D, Yeh CI, Burns S, Shapley RM. Laminar analysis of visually evoked activity in the primary visual cortex. *Proc Natl Acad Sci USA* 109: 13871–13876, 2012. doi:10.1073/pnas.1201478109.